ACKNOWLEDGEMENT

All praise to **ALMIGHTY ALLAH**, who provided me with the strength to accomplish this research. I am highly indebted to my supervisor Dr. Syed Zaheer Abbas for his worthy discussions, encouragement, inspiring guidance, remarkable suggestions, keen interest, constructive criticism & friendly discussions which enabled me to complete this research work.

Support from University of Engineering and Technology, Lahore, Pakistan is gratefully acknowledged. I am also thankful to University of Leeds, UK for providing the license of gPROMS model builder 4.1.0® and making this research possible.

ABSTRACT

In this work, one dimensional (1-D) non ideal plug flow mathematical model for the heterogeneous catalytic steam methane reforming (SMR) was developed in gPROMS model builder 4.1.0®, a software developed by Process System Enterprise (PSE). The required kinetic rate data in the model for various reforming catalysts was taken from literature. The developed reactor model was simulated and the modelling results were compared independently with the results from a software and also with the literature. The effect of key variables such as temperature, pressure, steam to carbon ratio (S/C) and gas mass flux (G_s) on the performance of the SMR process was studied and the modelling results were compared with an independent and well known equilibrium based software i.e. chemical equilibrium with applications (CEA) in terms of fuel and steam conversion, H_2 purity, H_2 yield (wt. % of CH_4) and selectivity of carbon based products. The modelling results were found in an excellent agreement with the equivalent equilibrium based results and the literature data. Later on, a comparative study was performed for various catalysts with their available kinetics to find out the most suitable catalyst and the operating conditions for the SMR process in an adiabatic fixed bed reactor.

TABLE OF CONTENTS

Acknowledgement II

Abstract III

Table of contents IV

List of figures VI

List of tables VII

Nomenclature VIII

1. Introduction 1

1.1 Uses of hydrogen 1

1.2 Hydrogen production processes 1

1.3 SMR process 2

1.4 Early kinetics studies of SMR 2

1.5 Early modelling studies of SMR 3

1.6 Problem statement 4

1.7 Research objectives 4

2. Mathematical modelling 5

3. Thermodynamic analysis of SMR 8

3.1 Published work describing thermodynamic analyisis of SMR 8

3.2 Model validation and thermodynamic analysis of SMR 8

3.2.1 Effect of temperature 9

3.2.2 Effect of pressure 9

3.2.3 Effect of feed ratio 11

3.3 Model validation under industrial scale conditions 12

3.4 Effect of G_s 14

4. Results and disussion 15

4.1 Performance of SMR process with various catalyts 15

4.1.1 Chosen catalysts 15

4.1.2 Comparison in terms of CH_4 conversion, H_2 yield and H_2 purity 16
4.1.3 Selectivity of C-based products 19
4.1.4 Thermal efficiency 21
5. Conclusion 23
6. References 24
7. Appendices 29
7.1 Appendix A 29
7.2 Appendix B 30

LIST OF FIGURES

Figure 3.1: Effect of temperature on a) CH_4 and H_2O conversion; b) H_2 yield (wt. % of CH_4) and H_2 purity at 1 bar and S/C of 3.0…….. 10

Figure 3.2: Effect of pressure on a) CH_4 and H_2O conversion; b) H_2 yield (wt. % of CH_4) and H_2 purity at 973 K and S/C of 3.0…….. 10

Figure 3.3: Comparison of model outputs with literature under the conditions mentioned in Table 3.3…..……..... 13

Figure 3.4: Dynamic profile of CH_4 and H_2 composition (dry basis) at the exit of reactor for various G_s, at 973 K, 30 bar and S/C of 3.0…….. 14

Figure 4.1: Comparison in terms of a) CH_4 conversion; b) H_2 yield (wt. % of CH_4); c) H_2 purity over various catalysts at 973 K, 1 bar, S/C of 3.0 and G_s of 3.5 kg m^{-2} s^{-1}……. 17

Figure 4.2: Rate of reaction of R1 as function of time over various catalysts at 973 K, 1 bar, S/C 3.0 and G_s of 3.5 kg m^{-2} s^{-1}…… 18

Figure 4.3: Temperature of gas as function of time over various catalysts at 973 K, 1 bar, S/C 3.0 and G_s of 3.5 kg m^{-2} s^{-1}……. 19

Figure 4.4: Comparison in terms of a) CH_4 selectivity; b) CO selectivity ; c) CO_2 selectivity at 973 K, 1 bar, S/C of 3.0 and G_s of 3.5 kg m^{-2} s^{-1}……. 20

Figure 4.5: Thermal efficiency of the reformer with various catalysts at 973 K, 1 bar, S/C of 3.0 and G_s of 3.5 kg m^{-2} s^{-1}……. 21

LIST OF TABLES

Table 2.1: Summary of mass, energy and momentum balance equations used in the reactor model…… 6

Table 3.1: Effect of S/C on CH_4 conversion, H_2 yield (wt. % of CH_4) and H_2 purity at 973 K and 1 bar…… 11

Table 3.2: Comparison of equilibrium compositions at the exit of the reformer from literature [45] and from our work……. 12

Table 3.3: SMR industrial operating conditions adopted from literature [32]……. 13

Table 3.4: Industrial output compositions on dry basis [32]…… 13

Table 4.1: Arrhenius kinetic parameters over various catalysts…….. 15

Table 4.2: Van't Hoff adsorption parameters for species…… 16

NOMENCLATURE

a_v	External surface area per unit volume of catalyst bed [$m^2\ m^{-3}$]
C_i	Concentration of i species [mol m^{-3}]
$C_{i,o}$	Initial concentration of species i in the gas phase [mol m^{-3}]
$C_{i,s}$	Concentration of species i in the solid phase [mol m^{-3}]
$C_{s,o}$	Initial concentration of species i in the solid phase [mol m^{-3}]
$C_{p,bed}$	Heat capacity of the catalyst bed [J $kg^{-1}\ K^{-1}$]
C_{pg}	Heat capacity of gases [J $kg^{-1}\ K^{-1}$]
D_i	Effective diffusion coefficient [$m^2\ s^{-1}$]
D_m	Average molecular diffusivity [$m^2\ s^{-1}$]
D_z	Axial dispersion coefficient [$m^2\ s^{-1}$]
d_p	Particle diameter [m]
E_j	Activation energy of reaction j [J mol^{-1}]
G	Gibbs free energy [J]
LHV_{H_2}	Lower heating value of H_2 [J mol^{-1}]
LHV_{CH_4}	Lower heating value of CH_4 [J mol^{-1}]
P_i	Partial pressure of species i [bar]
P	Total gas pressure [bar]
P_o	Initial pressure of the system [bar]
Pr	Prandtl number
ri	Rate of formation or consumption of species i [mol $kg_{cat}^{-1}\ s^{-1}$]
R_j	Rate of reaction j [mol $kg_{cat}^{-1}\ s^{-1}$]
R_g	Ideal gas constant [J $mol^{-1}\ K^{-1}$]
G_s	Gas mass flow velocity [kg $m^{-2}\ s^{-1}$]
ΔH_i	Heat of adsorption of i species [J mol^{-1}]
$H_{rxn,j}$	Heat of reaction of j reaction [J mol^{-1}]
h_f	Gas to solid heat transfer coefficient [W $m^{-2}\ s^{-1}$]
j_D, j_H	Chilton-Colburn factor for mass and heat transfer
$k_{g,i}$	Gas to solid mass transfer coefficient of component i [$m^3\ m^{-2}\ s^{-1}$]
k_j	Kinetic rate constant of reaction j
k_{oj}	Reference temperature dependent kinetic rate constant of reaction j
K_j	Thermodynamic equilibrium constant
K_i	Adsorption constant of species i

K_{oi}	Reference adsorption constant of species i
K_D	Viscous loss term in pressure drop calculations, Pa s^2 m^{-3}
K_V	Kinetic loss term in pressure drop calculations, Pa s^2 m^{-3}
Sc_i	Schmidt number
T	Gas temperature [K]
T_o	Gas inlet temperature [K]
T_s	Catalyst temperature [K]
$T_{s,o}$	Initial catalyst temperature [K]
u	Superficial velocity of the gases [m s^{-1}]
z	Axial dimension [m]
Re	Reynolds number

Greek letters

Ω	Unit less dominator term in the reaction kinetics
ε_b	Packing bed porosity
η_j	Effectiveness factor of reaction j
λ_g	Average gas thermal conductivity [W m^{-1} K^{-1}]
λ_s	Solid thermal conductivity [W m^{-1} K^{-1}]
λ_z^f	Effective thermal conductivity [W m^{-1} K^{-1}]
μ_g	Average gas viscosity [kg m^{-1} s^{-1}]
ρ_{bed}	Density of the catalyst bed [kg m^{-3}]
ρ_{cat}	Density of the catalyst pellet [kg m^{-3}]
ρ_f	Fluid density [kg m^{-3}]

1. INTRODUCTION

High energy consumption, finite fossil fuel reserves and environmental concerns impel the research community to search for efficient and environment friendly alternatives to meet our increasing energy demands [1]. Because of their continuous depletion, limited nature and non-homogeneous distribution, fossil fuels are getting scarce and their prices are gearing up [2]. Therefore, we are in dire need to shift away from carbon dioxide intensive processes and to switch to a non-fossil fuel energy source [3]. In this context, hydrogen (H_2) emerges as a clean energy fuel and it has received great interest as a green fuel recently [4]. Without polluting the environment, H_2 can be used directly to drive the internal combustion (IC) engines or indirectly to generate electricity using fuel cells [1]. H_2 has wide range of applications industrially, domestically and in space technology [5]. At present, H_2 is predominantly employed in petroleum refining and petrochemicals, fertilizer industry, methanol production and somewhat to a lesser extent in metal refining [6].

1.1 USES OF HYDROGEN

Primarily, H_2 is being consumed for ammonia and other nitroginated fertilizers synthesis, hydrocracking and hydrotreating processes. It is also used for hydrogenation of food and hazardous wastes, synthesis of alcohols and ethers, gas to liquid synthesis technology (GTL), rocket fuel and also as a potential fuel in IC engines and industrial furnaces [7]. The advantages of H_2 include: high energy conversion efficiency, availability, easy transportation, an ease of conversion to other forms, high gross and net calorific values than most of the conventional fuels such as; methane (CH4), gasoline, diesel and coal [2]. Combustion of H_2 only produces water vapors without the emission of any greenhouse gas [8].

1.2 HYDROGEN PRODUCTION PROCESSES

The processes used for H_2 production are conventional thermochemical technologies (gasification, pyrolysis, reforming, thermochemical cycle), conventional electrochemical technologies (electrolysis, cold/hot plasma, photo electrochemical) and biological/biochemical technologies (photosynthetic and fermentative) [9]. Approximately, 90 % of worldwide H_2 energy is derived from fossil-fuels such as; natural gas (NG), coal and crude oil [10]. NG, naphtha, petroleum coke, coal, water and ammonia are common feedstocks used for H_2 production but currently NG is the dominant source [11]. The various routes available for H_2 production by using NG include SMR, partial oxidation (POx) and autothermal reforming

(ATR). Despite its negative impact on environment and contribution to global warming through emission of greenhouse gases, SMR is still considered to be the dominant process to produce H_2. Presently, this process contributes to almost 50 % of world's H_2 produced [12-14].

1.3 SMR PROCESS

The conventional SMR process comprises two main steps, the first step proceeds with the conversion of CH_4 to H_2 in a conventional reformer where endothermic SMR reaction (R1) occurs at an elevated temperature (800-1000 ^oC) and mild pressure (20-35 atm), followed by the second step of lower temperature (200-400 ^oC) conversion of carbon monoxide to H_2 via slightly exothermic water-gas shift (WGS) reaction (R2) taking place at a medium pressure (10-15 atm) [15].

$$CH_{4(g)} + H_2O_{(g)} \rightleftharpoons CO_{(g)} + 3H_{2(g)} \qquad \Delta H_{rxn,298K} = 206.3\ kJ\ mol_{CH_4}{}^{-1} \qquad \text{(R1)}$$

$$CO_{(g)} + H_2O_{(g)} \rightleftharpoons CO_{2(g)} + H_{2(g)} \qquad \Delta H_{rxn,298K} = -41.1\ kJ\ mol_{CO}{}^{-1} \qquad \text{(R2)}$$

R1 is strongly endothermic in nature and it is favoured at high temperature while R2 is more sensitive to lower temperatures. The net reaction is highly endothermic and it requires external heating to take place. The global SMR reaction is given as [16];

$$CH_{4(g)} + 2H_2O_{(g)} \rightleftharpoons CO_{2(g)} + 4H_{2(g)} \qquad \Delta H_{rxn,298K} = 164.9\ kJ\ mol_{CH_4}{}^{-1} \qquad \text{(R3)}$$

SMR is a quite complex process and numerous efforts have been made in recent years aiming at the development of the most suitable catalyst to maximize the production of syngas from this process [17]. It is very difficult to give a specific order of catalytic activity and selectivity for SMR process. Jones et al. [18] proposed the following catalytic activity order: Ruthenium (Ru) > Rhodium (Rh) > Iridium (Ir) > Platinum (Pt), indicating Pt as the least active metal as compared to others. Although, these noble metals are highly active and have less carbon deposition ability, the nickel (Ni) catalyst is so far the best and most commonly used catalyst at industrial scale for SMR process [19]. Ni presents high activity, low attrition and it is expensive in comparison to some other available choices, but it can be recouped by using lower Ni content [20].

1.4 EARLY KINETICS STUDIES OF SMR

The performance of the SMR process and product distribution is influenced by several factors including operating conditions (T, P, S/C), catalyst type and reformer design features. Many

studies have been carried out to investigate the kinetics of SMR reactions. The first extensive kinetic study was performed using Ni catalyst supported on kieselguhr at atmospheric pressure and in the temperature range of 335-635 ^{o}C. There was no mechanism suggested, but it was concluded that both CO and CO_2 were primary reaction products [21]. Numaguchi and Kikuchi [22] determined the intrinsic kinetics of SMR process in an integral reactor which was considered to be a fixed bed model and suggested that the surface reactions were the rate determining steps (RDS) with only CO as a primary reaction product. Xu and Froment [23] developed a kinetic model for SMR over spinel $Ni/MgAl_2O_4$ catalyst at 500-670 ^{o}C, and surface reactions were considered to be the RDS in the mechanism proposed. Soliman et al. [24] studied the intrinsic kinetics of SMR over a nickel/calcium aluminate catalyst. They proposed a mechanism similar to Xu and Froment [23] but with CO_2 as primary product which is then converted to CO by the reverse R2. A kinetic model for SMR in the temperature range of 500-600 ^{o}C, was proposed by Luna and Becerra [25] over a commercial Ni on alumina-titania catalyst. Hou and Hughes [26] performed experiments to study the kinetics of SMR and the reverse R2 by using $Ni/\alpha\text{-}Al_2O$ catalyst in the temperature range of 475-550 ^{o}C and under the conditions of no diffusion limitation. A kinetic model was proposed with surface reactions to be the RDS.

1.5 EARLY MODELLING STUDIES OF SMR

The SMR is a mature technology and there exist several models in the literature for SMR reactors ranging from pseudo-homogeneous to heterogeneous models, operated in steady-state and dynamic way. The SMR model development began in 1960s. McGreavy and Newmann [27] proposed a steady-state SMR model of a top-fired reformer and compared the outputs of the model with the plant data. Later, they modified the model for dynamic simulation. Singh and Saraf [28] developed a 1-D steady-state homogeneous SMR model for a side-fired furnace and modified it for un-steady state simulation. Xu and Froment [29] used the kinetics that accounted for diffusional limitations in a 1-D heterogeneous model to simulate a commercial reformer. Soliman et al. [30] used the kinetic rate expressions from Xu and Froment [23] to develop a 1-D heterogeneous model and the model performance was tested against the industrial reformers. Murty and Murthy [31] formulated a model of a top-fired reformer, the model was tested against the operating reformer data for the purpose of validation and the sensitivity analysis was performed to identify the key variables affecting the performance of SMR reformer. Plehiers and Froment [32] developed a 1-D heterogeneous model for side-fired

SMR reformer, which was validated with industrial results and had the ability to predict temperature distribution and effluent composition in furnace. Recently, Yu et al. [33] performed 1-D pseudo-homogeneous modeling, compared the simulation result with the operating reformer data and optimized the performance of reformer. Shayegan et al. [34] developed a rigorous 2-D mathematical model, investigated the steady-state operation of an industrial Midrex™ reformer and compared the outputs of 1-D and 2-D models. They also explained how catalyst loading profile affects the reformer performance. Ebrahimi et al. [35] validated the model of a top fired NG reformer against the industrial and literature data, and investigated the effect of important process variables on the performance of SMR reformer. Olivieri and Vegliò [36] used 1-D pseudo-homogeneous model to simulate a side-fired reformer in hydrogen plant, optimized the tube skin temperature for maximum catalytic tube life, and optimum fuel distribution among burners was evaluated to achieve the desired conversion.

1.6 PROBLEM STATEMENT

Industrialization and population growth has led to a surge in the global demand for energy in past few years and conventional fuels such as NG, coal and crude oil are constant threat to our environment. H_2 has potential to meet requirements in that quest. The SMR process needs more maturity for efficient H_2 production and good choice of catalyst is a cornerstone of this process. The present work provides the comparison of different catalysts performance for H_2 production by using kinetics available in the literature.

1.7 RESEARCH OBJECTIVES

- Development of 1-D heterogeneous reactor model using gPROMS.
- Simulation of the SMR model to study the effect of temperature (T), pressure (P), steam to carbon ratio (S/C) and space velocity on the performance of SMR in a packed bed reactor.
- Validation of the developed model.
- Comparison of the performance of various catalysts in terms of CH_4 conversion, H_2 purity, H_2 yield (wt. % of CH_4), selectivity of C-based products and thermal efficiency of SMR process.

2. MATHEMATICAL MODELLING

A 1-D heterogeneous mathematical model is constructed to study the performance and behaviour of SMR process at dynamic and steady state conditions by considering the transfer of heat and mass in both fluid and solid phases. The differential mass, heat and momentum balances as function of time and axial position along the length of the reactor are taken into account in the development of the model. The basic assumptions of the model are;

a) The flow pattern is assumed to be non-ideal plug flow.
b) Ideal gas behavior is applicable.
c) The operation is considered to be adiabatic in nature.
d) Bed porosity is constant and size of the catalyst particles is uniform.
e) Radial variations in concentration and temperature gradient have been neglected i.e. heat and mass flow pattern is only studied in axial direction.
f) The effect of carbon deposition is not considered in this work.
g) No axial mixing but perfect radial mixing within the reactor.
h) Isothermal behavior is considered within the catalyst particles.

Involvement of several reactions makes SMR a complex process. To minimize the complexity in the model, only those reactions with appreciable kinetic rates and consequently affecting the overall process are being considered. Steam methane reforming reaction (R1), global steam methane reforming reaction (R3) and WGS reaction (R2) are considered to model the reactor. The rate equations for these reactions are given in Appendix A.

The mathematical equations for mass, energy and momentum balances to model the SMR process are given in Table 2.1.

The inlet and exit boundary conditions to solve the equations of the reactor model are:

At the reactor inlet (z = 0)

$$C_i = C_{i,0}; \quad T = T_0; \quad T_s = T_{s,0}; \quad P = P_0$$

At the reactor outlet (z = L):

$$\frac{\partial C_i}{\partial z} = 0; \quad \frac{\partial T}{\partial z} = 0; \quad \frac{\partial T_s}{\partial z} = 0$$

Initial conditions:

$$C_i = C_{i,0}; \quad T = T_0; \quad T_s = T_{s,0}$$

Table 2.1

Summary of mass, energy and momentum balance equations used in the reactor model

Gas phase mass and energy balance

$$\varepsilon_b\left(\frac{\partial C_i}{\partial t}\right)+\frac{\partial(uC_i)}{\partial z}+k_{g,i}a_v(C_i-C_{i,s})=\varepsilon_b D_z\frac{\partial^2 C_i}{\partial z^2}$$

$$\varepsilon_b\rho_g C_{pg}\left(\frac{\partial T}{\partial t}\right)+u\rho_g C_{pg}\frac{\partial(T)}{\partial z}=h_f a_v(T_s-T)+\lambda_z^f\frac{\partial^2 T}{\partial z^2}$$

Solid phase mass and energy balance

$$k_{g,i}a_v\left(C_i-C_{i,s}\right)=(1-\varepsilon_b)\rho_{cat}r_i$$

$$\rho_{bed}C_{p,bed}\left(\frac{\partial T_s}{\partial t}\right)+h_f a_v(T_s-T)=(1-\varepsilon_b)\rho_{cat}\sum -\Delta H_{rxn,j}\eta_j R_j$$

Pressure drop

$$\frac{\Delta P g_c}{L}=-K_D u-K_V u^2$$

with;

$$K_D=\frac{150\mu(1-\varepsilon_b)^2}{d_p^2\varepsilon_b^3};\ K_V=\frac{1.75(1-\varepsilon_b)\rho_g}{d_p\varepsilon_b^3}$$

The equilibrium and kinetic rate constants are presented in Appendix A. The values of Arrhenius kinetic parameters and and Van't Hoff adsorption parameters for species over various catalysts obtained from literature are presented in Table 4.1 and Table 4.2, respectively. The empirical correlations used to determine the physical properties are listed in Appendix B.

Rates for the disappearance and formation of species involved in the reactor system are obtained as follows;

$$r_{CH_4}=-\eta_1 R_1-\eta_3 R_3 \quad (2.1)$$

$$r_{H_2O}=-\eta_1 R_1-\eta_2 R_2-2\eta_3 R_3 \quad (2.2)$$

$$r_{CO}=\eta_1 R_1-\eta_2 R_2 \quad (2.3)$$

$$r_{H_2}=3\eta_1 R_1+\eta_2 R_2+4\eta_3 R_3 \quad (2.4)$$

$$r_{CO_2}=\eta_2 R_2+\eta_3 R_3 \quad (2.5)$$

In the reactor model, partial differential algebraic equations (PDAE's) are involved, and these equations are solved by gPROMS. PDAEs subjected to the initial and boundary conditions given above are solved by the finite difference method. gPROMS used differential algebraic solver (DASOLV) for the transformation of nonlinear partial differential equations (PDEs) to

ordinary differential equations (ODEs) and then the system of these transformed ODEs was solved by fourth order Runge Kutta method.

CEA, a software which performs equilibrium calculations by using approach of minimizing the Gibbs free energy, was used to obtain the equilibrium compositions of species participating in the reaction [37-39]. The results generated with CEA were compared with the results from our model.

3. THERMODYNAMIC ANALYSIS OF SMR

The optimal operating conditions for the SMR process can be obtained by performing sensitivity analysis while taking into account all the variables affecting the performance of the SMR process. R1 and R2 are considered to be sufficient to illustrate the thermodynamic equilibrium of SMR process [40] . Although, Xu and Froment [23] explained that the global reaction (R3) is also necessary to represent the experimental kinetic rate data.

3.1 PUBLISHED WORK DESCRIBING THERMODYNAMIC ANALYISIS OF SMR

A substantial amount of work has been published describing the thermodynamic analysis of SMR process [41-43]. The Gibbs free minimization and entropy maximization methods can be used to determine the equilibrium product distribution and equilibrium temperature, respectively [41]. The two criteria to determine the equilibrium composition of a system at a fixed temperature and pressure are: the total Gibbs free energy is at minimum in respect of all possible changes (ii) the differential of total Gibbs free energy is zero [44]. Lutz et al. [45] computed the equilibrium compositions at the outlet of reformer by employing CHEMKIN software, with temperature range of 500-1000 ^{o}C, S/C of 2-4 and pressure of 10 atm. Seo et al. [46] employed Aspen Plus™ software to study the effect of temperature in the range 500 – 800 ^{o}C on equilibrium composition with reactor pressure of 1 bar and S/C of 1. Ávila-Neto et al. [40] performed simulation to obtain the equilibrium compositions and validated the results against the published data. Farshad et al. [47] studied the thermodynamic analysis of SMR process by employing Gibbs energy minimization method for syngas production in the temperature range 600 – 1200 K, pressure 1 – 30 bar and S/C of 0.5 - 3.

3.2 MODEL VALIDATION AND THERMODYNAMIC ANALYSIS OF SMR

In our present work, the developed model was first simulated at equilibrium conditions to perform the thermodynamic analysis and for the validation against the equilibrium data obtained from CEA model. In order to carry out the thermodynamic analysis, the gaseous species, which are considered to be present in the reaction mixture are CH_4, CO, H_2, H_2O, CO_2 and N_2. To examine the effect of temperature both pressure and ratio of feedstock were fixed. The effect of pressure was investigated by keeping the temperature and feedstock ratio at a constant value. Similarly, the effect of S/C ratio on product distribution was investigated at a

fixed temperature and pressure. Following equations were used to calculate the fuel conversion, H_2 yield and purity.

$$CH_4\ Conversion\ [\%] = \frac{(n_{CH4.in} - n_{CH4,out})}{n_{CH4,in}} \times 100 \tag{3.1}$$

$$H_2\ Purity\ [\%] = \frac{n_{H2,out}}{(n_{H2,out} + n_{CH4,out} + n_{CO,out} + n_{CO2,out})} \times 100 \tag{3.2}$$

$$H_2\ Yield\ [wt.\%\ of\ CH_4] = \frac{(mol.\ weight\ of\ H_2 \times n_{H2,out})}{(mol.\ weight\ of\ CH_4 \times n_{CH4,in})} \times 100 \tag{3.3}$$

3.2.1 EFFECT OF TEMPERATURE

Temperature plays an important role towards the sensitivity of the SMR process. At equilibrium, when the system is subjected to an increase in temperature, there is an increase in the rate of SMR reaction (R1) according to Le Chatelier's principle. In Fig. 3.1(a-b), the effect of temperature on feed conversion, H_2 yield and H_2 purity is shown. The mean relative error between the results of our model and those of generated with CEA is 1.95% showing that our model is in good agreement with CEA model. It is clear that CH_4 conversion increases gradually up to a certain peak value but with further increase in temperature it does not change and stays there. The increase in CH_4 conversion is from 20.9% to 96.4% as the temperature rises from 673 to 973 K. With further increase of 300 K, there is only 3.7 % increase in CH_4 conversion. The rate of disappearance of CH_4 is proportional to H_2 yield and purity. The effect of temperature on H_2 yield and purity is exhibited in Fig. 3.1(b). It can be inferred that the H_2 purity increases as the temperature raises from 673 to 1023 K. As temperature is increased beyond 1023 K, a drop in H_2 purity is recorded. It is due to the reverse R2 which decreases steadily the H_2 purity, although CH_4 conversion remains still maximum at such a high temperature. The H_2 purity varies from 45.5 % to 77 % as the temperature increases from 673 to 1023 K and it drops down to 76.4 % at 1273 K. It is evident from Fig. 3.1 (b) that H_2 yield grows rapidly in the temperature interval of 673-973 K and it attains a value of 42 % at 973 K. From 1073-1273 K H_2 yield doesn't vary appreciably and it drops down to 40.8 % at 1273 K.

3.2.2 EFFECT OF PRESSURE

To investigate the effect of pressure on feed conversion, H_2 yield and purity, a temperature condition of 973 K with S/C of 3 is used. Fig. 3.2(a) shows that the lower pressure favors the fuel conversion.

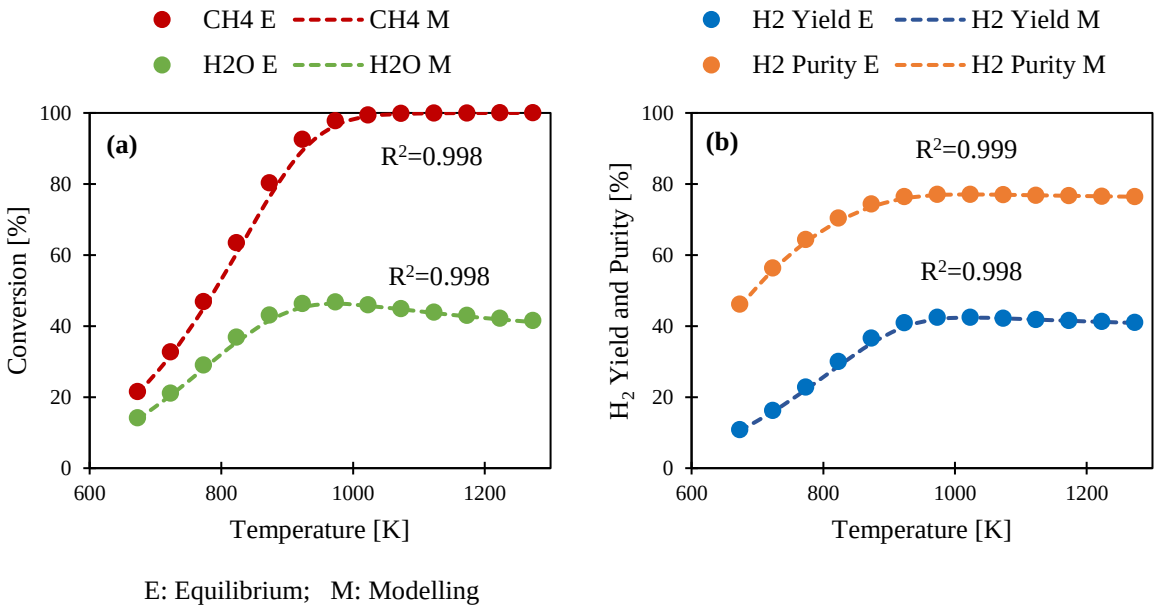

Fig. 3.1. Effect of temperature on a) CH_4 and H_2O conversion; b) H_2 yield (wt. % of CH_4) and H_2 purity at 1 bar and S/C of 3.0.

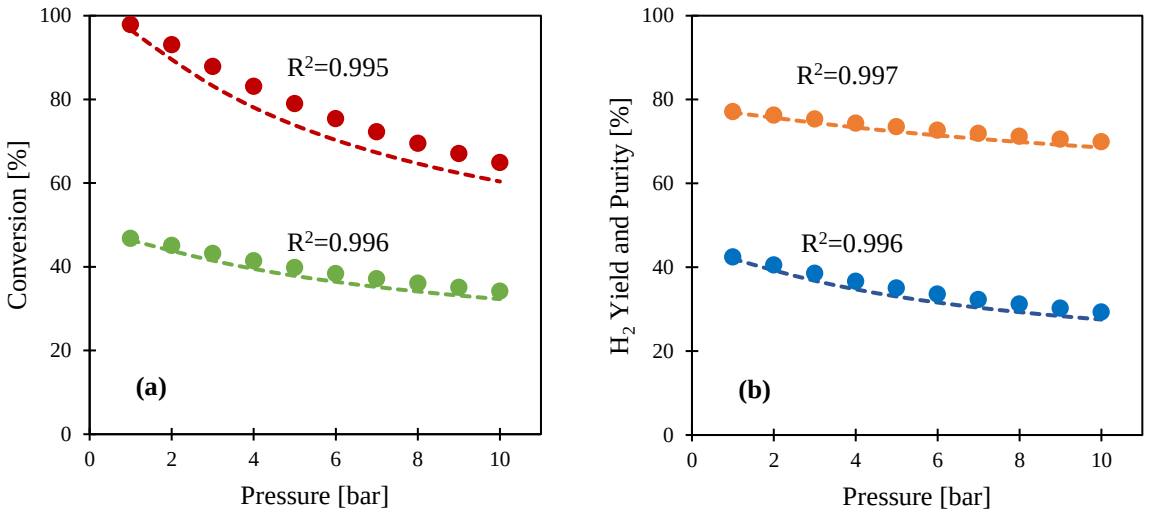

Fig. 3.2. Effect of pressure on a) CH_4 and H_2O conversion; b) H_2 yield (wt. % of CH_4) and H_2 purity at 973 K and S/C of 3.0.

High pressure shifts the equilibrium towards the reactants in SMR reaction because of having larger number of moles on the product side which in turn results in lower CH_4 conversion. On the other hand, R2 is equimolar and thus impervious to any change in pressure once the equilibrium is established. The decrease in CH_4 conversion in SMR is from 96.6 % to 60.4 % as the pressure is raised from 1 to 10 bar. In Fig. 3.2(b), the effect of pressure on H_2 purity is presented, showing a decrease of 10.8 % in purity when the pressure is increased from 1 to 10 bar. It is also clear from Fig. 3.2(b) that the H_2 yield drops from a value of 42% at 1 bar to 27.5

% at 10 bar.

3.2.3 EFFECT OF FEED RATIO

The choice of optimum S/C is of paramount importance which in turn effects the overall performance of the SMR process. Higher S/C tends to shift R1 in forward direction resulting in increased production of H_2 due to an increase in overall conversion of CH_4. A comparison between modelling and equilibrium results is presented in Table 3.1.

Table 3.1

Effect of S/C on CH_4 conversion, H_2 yield (wt. % of CH_4) and H_2 purity at 973 K and 30 bar

S/C	CH_4 Conversion [%]	H_2 Yield [wt. % of CH_4]	H_2 Purity [%]
1	M: 71.7 E: 76.8	M: 28.3 E: 30.0	M: 69.2 E: 70.4
2	M: 90.9 E: 94.1	M: 38.0 E: 39.1	M: 75.1 E: 75.6
3	M: 96.6 E: 97.8	M: 42.0 E: 42.4	M: 76.9 E: 77.1
4	M: 98.5 E: 99.0	M: 44.1 E: 44.2	M: 77.7 E: 77.8
5	M: 99.3 E: 99.5	M: 45.3 E: 45.3	M: 78.2 E: 78.2
6	M: 99.6 E: 99.7	M: 46.1 E: 46.0	M: 78.5 E: 78.5

Excess of steam favors CH_4 conversion which enhances the production of H_2 and lessen the chances of coke deposition. Tabulated results show that the effect of S/C on fuel conversion, H_2 yield and purity is more pronounced in the range 1-3. Higher S/C results in more production of CO_2 and hence improves H_2 purity. Modelling results exhibit an increase of 34.7 %, 48.4 % and 11.1 % when S/C is increased from 1 to 3 but with further increase from 3 to 6 in S/C there is only an increase of 1.1 %, 4.5 % and 1 % in CH_4 conversion, H_2 yield and H_2 purity, respectively. It is obvious from the results that whenever higher fuel conversion, yield and purity is desired, steam must be used in excess although this will results in an increase of overall

operational cost of the process. The optimum S/C is always a compromise between the overall efficiency and overall operational cost of the process. On an industrial scale, a feed ratio of 3 is commonly used in SMR processes.

After validation of model outputs against CEA results, the modeling results are also compared with literature data. Table 3.2 shows the comparison of our model outputs with literature [45] and a mean relative error of 5.90 % is found, showing that the model outputs are also in good agreement with the literature results.

Table 3.2

Comparison of equilibrium compositions at the exit of the reformer from literature [45] and from our work

Operating Conditions	Components	773 K		873 K		973 K		1073 K		1173 K		1273 K	
		This work	Liter.	This work	Liter.	This work	Liter.	This work	Liter.	This work	Liter.	This work	Liter.
P=10 atm S/C=2	CH_4	0.263	0.260	0.209	0.203	0.142	0.126	0.075	0.050	0.028	0.015	0.007	0.004
	CO	0.002	0.004	0.014	0.015	0.049	0.061	0.101	0.115	0.145	0.153	0.168	0.168
	H_2	0.167	0.174	0.285	0.300	0.410	0.434	0.518	0.563	0.588	0.610	0.615	0.625
	H_2O	0.528	0.524	0.432	0.421	0.334	0.314	0.252	0.222	0.201	0.184	0.182	0.176
	CO_2	0.040	0.038	0.060	0.061	0.065	0.065	0.053	0.050	0.038	0.038	0.028	0.027

3.3 MODEL VALIDATION UNDER INDUSTRIAL SCALE CONDITIONS

After validation of our model at equilibrium, it is further validated with steady state industrial data away from equilibrium. Operating conditions used to simulate our model are adopted from Plehiers and Froment [32] and presented in Table 3.3. It is evident from Table 3.4 and Fig. 3.3 that the simulation results from our model are in good agreement with the plant data and simulated results from Plehiers and Froment [32].

Table 3.3

SMR industrial operating conditions adopted from literature [32]

Pressure [P]	29 bar
Gas feed temperature [T]	760 °C
Catalyst temperature [T_s]	760 °C
Inlet mole fractions	
CH_4	0.2128
H_2	0.0260
H_2O	0.7144
CO_2	0.0119
N_2	0.0350

Table 3.4

Industrial output compositions on dry basis [32]

Components	**Plant data** [32]
CH_4	10.25 – 10.80
CO	8.20 - 8.70
H_2	64.50 - 65.40
CO_2	10.52 - 10.80
N_2	5.00 – 5.65

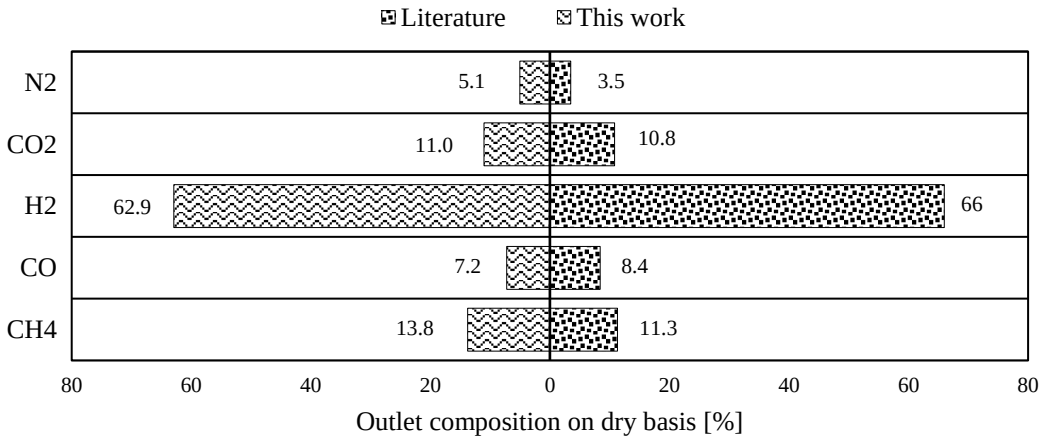

Fig. 3.3. Comparison of model outputs with literature under the conditions mentioned in Table 3.3

3.4 EFFECT OF G_S

The gas mass flow velocity (G_s) is also one of the important operating parameter affecting the performance of SMR process. The choice of the most suitable G_s depends upon the length of the reformer. To obtain the CH_4 conversion close to an equilibrium value, a velocity of (1.5 - 2 m s^{-1}) can be used [48]. The performance of the SMR process is checked with various values of G_s.

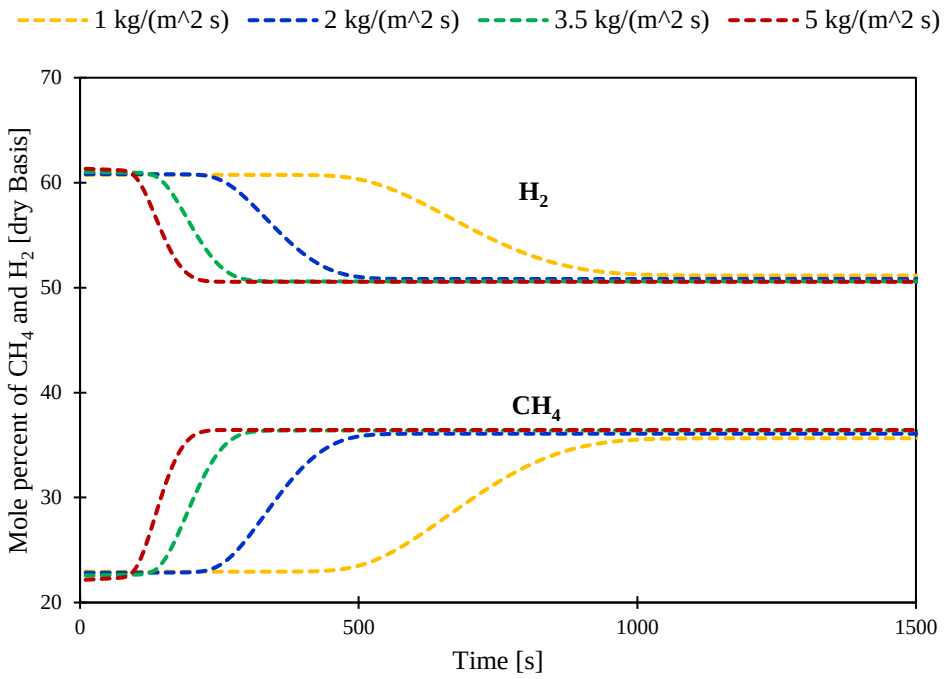

Fig. 3.4. Dynamic profile of CH_4 and H_2 composition (dry basis) at the exit of reactor for various G_s, at 973 K, 30 bar and S/C of 3.0.

In Fig. 3.4, the dynamic variation of H_2 and CH_4 composition on dry basis at the outlet of the reactor under the fixed operating conditions of 973 K, 30 bar, S/C of 3 and various G_s (1 – 5 kg m^{-2} s^{-1}) is presented. The lower G_s results in longer residence time with smaller mole percent of CH_4 in the effluent stream which means higher CH_4 conversion is achieved. For a G_s of 1 kg m^{-2} s^{-1}, the conversion of CH_4 is 43.7 % which is very close to equilibrium value of 44.3 % under the identical operating conditions. As G_s is increased, a decrease in CH_4 conversion is observed because of having smaller residence time in the reactor. The optimum G_s selected is 3.5 kg m^{-2} s^{-1} because of having a CH_4 conversion and H_2 purity of 41.5 % and 60.7 % respectively, corresponding to 44.3 % and 62.1 % at equilibrium. G_s of 3.5 kg m^{-2} s^{-1} is opted because at this value, higher CH_4 conversion can still be achieved by staying away from equilibrium as equilibrium is not desired.

4. RESULTS AND DISUSSION

4.1 PERFORMANCE OF SMR PROCESS WITH VARIOUS CATALYTS

After validation of the developed model, the performance of SMR process is checked by implementing the kinetics available in literature to our developed model.

4.1.1 CHOSEN CATALYSTS

For this purpose, a set of catalysts, comprising of 11 various catalysts, with available kinetics presented in Table 4.1 and Table 4.2, is chosen. Xu and Froment [23] used a commercial nickel catalyst with 15.2 % nickel content supported on magnesium spinel (Catalyst-1) and developed a general intrinsic kinetic model with rate equations (A.1-A.4). Soliman et al. [24] studied the intrinsic kinetics of SMR over a nickel calcium aluminate catalyst (Catalyst-2) and a mechanism similar to Xu and Froment [23] was suggested. Hou and Hughes [26] used a commercial Ni/Al_2O_3 with NiO content of 15-17 % (Catalyst-3) and developed a kinetic model with rate equations (A.5-A.8).

Table 4.1
Arrhenius kinetic parameters over various catalysts

Reference	E_1 (J/mol)	E_2 (J/mol)	E_3 (J/mol)	$k_{o,1}$ (mol/(kg_{cat} s))	$k_{o,2}$ (mol/(kg_{cat} s))	$k_{o,3}$ (mol/(kg_{cat} s))
[23]	240,100	67,130	243,900	1.17×10^{15} $bar^{0.5}$	5.43×10^{5} bar^{-1}	2.83×10^{14} $bar^{0.5}$
[24]	-	32,520	185,592	-	4.08×10^{4} bar^{-1}	1.19×10^{12} $bar^{0.5}$
[26]	209,200	15,400	109,400	1.87×10^{11} $bar^{0.25}$	6.03×10^{-3} bar	3.46×10^{5} $bar^{0.25}$
[49]	209,500	70,200	211,500	9.048×10^{11} $bar^{0.5}$	5.43×10^{5} bar^{-1}	2.14×10^{9} $bar^{0.5}$
[50]	218,550	73,523	236,850	5.83×10^{11} $bar^{0.5}$	2.51×10^{4} bar^{-1}	4.67×10^{13} $bar^{0.5}$
[51]	217,010	68,200	215,840	5.79×10^{12} $bar^{0.5}$	9.33×10^{6} bar^{-1}	1.29×10^{13} $bar^{0.5}$
[52]	83,800	15,100	89,200	1.62×10^{7} $bar^{0.5}$	2.34×10^{7} bar^{-1}	4.55×10^{7} $bar^{0.5}$
[53]	216,722	67,966	227,941	9.78×10^{14} $bar^{0.5}$	5.29×10^{5} bar^{-1}	2.57×10^{14} $bar^{0.5}$
[54]	240,100	-	209,754	4.13×10^{13} $bar^{0.5}$	-	8.29×10^{11} $bar^{0.5}$
[54]	247,303	-	265,851	4.88×10^{14} $bar^{0.5}$	-	1.17×10^{15} $bar^{0.5}$
[55]	257,010	89,230	236,700	5.19×10^{12} $bar^{0.5}$	9.90×10^{6} bar^{-1}	1.32×10^{13} $bar^{0.5}$

Hoang et al. [49] determined the kinetics of SMR over sulfide nickel catalyst with 9.8 % nickel on a gamma alumina support (Catalyst-4) and used kinetic model from Xu and Froment to fit the experimental data. Oliveira et al. [50, 51] determined the true kinetics of SMR over commercial Ni/Al_2O_3 catalyst (Catalyst-5) and a pre-commercial Ni/Al_2O_3 catalyst (Catalyst-6) with 15.4 % and 10 % nickel content respectively while kinetic model from Xu and Froment [23] was used to implement these derived kinetics to develop a mathematical model.

Table 4.2

Van't Hoff adsorption parameters for species

Reference	K_{o,CH_4} $(bar)^{-1}$	$K_{o,CO}$ $(bar)^{-1}$	K_{o,H_2} $(bar)^{-1}$	K_{o,H_2O} $(bar)^{-1}$	K_{o,CO_2} $(bar)^{-1}$	ΔH_{CH_4} (J/mol)	ΔH_{CO} (J/mol)	ΔH_{H_2} (J/mol)	ΔH_{H_2O} (J/mol)	ΔH_{CO_2} (J/mol)
[23]	6.65×10^{-4}	8.23×10^{-5}	6.12×10^{-9}	1.77×10^{5} bar	-	-38,280	-70,650	-82,900	88,680	-
[24]	-	2.90	-	6×10^{4} bar	-	-	-19,813	-	54,340	-
[26]	-	5.13×10^{-11}	5.68×10^{-9} $(bar)^{0.5}$	9.25 bar	-	-	-140,000	-93,400	15,900	-
[49]	1.995×10^{-3}	8.11×10^{-5}	7.05×10^{-9}	1.68×10^{4} bar	-	-36,650	-70,230	-82,550	85,770	-
[50]	6.65×10^{-4}	8.23×10^{-5}	6.12×10^{-9}	1.77×10^{5} bar	-	-38,280	-70,650	-82,900	88,680	-
[51]	6.65×10^{-4}	8.23×10^{-5}	6.12×10^{-9}	1.77×10^{5} bar	-	-38,280	-70,650	-82,900	88,680	-
[52]	1.49×10^{-6}	2.34×10^{-6}	3.88×10^{-5}	2.91×10^{8} bar	8.33×10^{-8}	-98,800	-111,200	-88,200	112,300	-115,600
[53]	9.58×10^{-4}	8.09×10^{-5}	6.20×10^{-9}	1.68×10^{5} bar	-	35,773	-70,187	-82,643	87,743	-
[54]	1.09×10^{-3}	-	-	1.04×10^{6} bar	-	-34,835	-	-	98,435	-
[54]	2.82×10^{-4}	-	-	1.23×10^{6} bar	-	-44,022	-	-	100,208	-
[55]	6.65×10^{-4}	8.23×10^{-5}	6.12×10^{-9}	1.77×10^{5} bar	-	-38,280	-70,650	-82,900	88,680	-

Halabi et al. [52] used $Rh/Ce_{0.6}Zr_{0.4}O_2$ (Catalyst-7) in an integral fixed bed reactor to determine the true kinetics of SMR with rate equations (A.9-A13). Kinetics of SMR over Ni/Al_2O_3 with nickel content of 10.34 % (Catalyst-8) were determined in an adiabatic fixed bed reactor by Kanhari et al. [53]. Obradović et al. [54] performed the intrinsic kinetic of study of SMR on commercial Ni based catalyst with nickel content of 11.8 % (Catalyst-9) and on commercial $Pt/Ni/Al_2O_3$ (Catalyst-10). Kinetics of SMR over $NiO/\alpha\text{-}Al_2O_3$ catalyst with 18% nickel content (Catalyst-11) were studied by Abbas et al. [55] to perform a modelling study in a plug flow reactor.

4.1.2 COMPARISON IN TERMS OF CH_4 CONVERSION, H_2 YIELD AND H_2 PURITY

G_s plays an important role to achieve equilibrium. Here, our goal is not to achieve equilibrium

but to stay away from equilibrium and to evaluate the performance of different chosen catalysts on the basis of feed conversion, H_2 yield, purity and selectivity of C-based products. To achieve this, a G_s value of 3.5 kg m^{-2} s^{-1} is chosen because at this value our model gives results close to equilibrium but still far enough from equilibrium range.

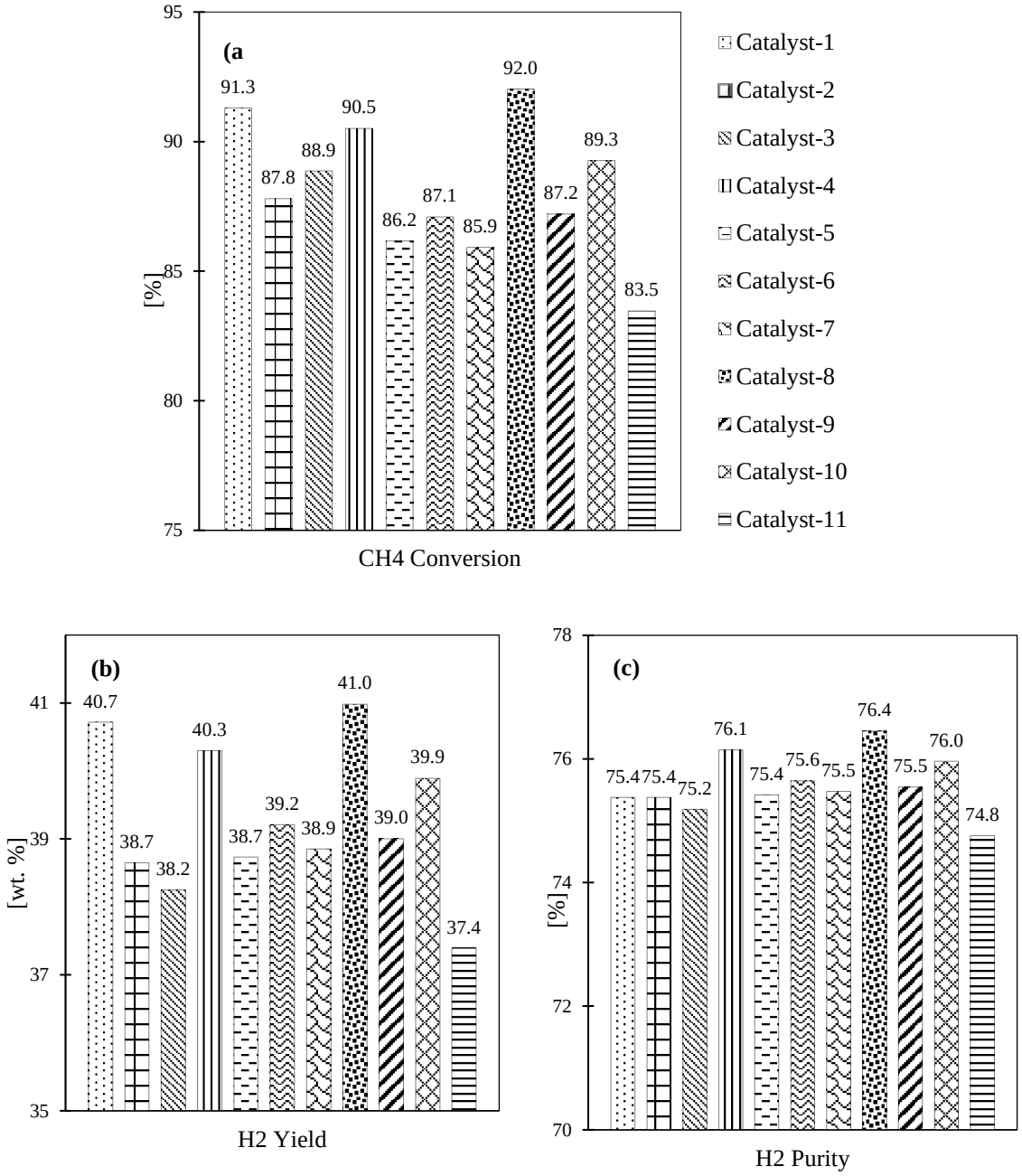

Fig. 4.1. Comparison in terms of a) CH_4 conversion; b) H_2 yield (wt. % of CH_4); c) H_2 purity over various catalysts at 973 K, 1 bar, S/C of 3.0 and G_s of 3.5 kg m^{-2} s^{-1}.

In Fig. 4.1(a), the conversion of CH_4 at the exit of the reformer with different catalysts used is presented. Catalyst-8 which is a nickel based catalyst gives a highest CH_4 conversion of 92 % because of its very fast kinetics. Activation energy for R1 with catalyst-8 is smaller and the

value of rate constant is larger due to which rate of disappearance of CH_4 with catalyst-8 is much higher as compared to other catalysts. Fig. 4.2 shows the rate of reaction of R1 with various catalysts as a function of time in the middle of the reactor. It can be observed that the highest peak for the rate of SMR reaction is observed when the reformer is loaded with catalyst-8 and it gives the highest CH4 conversion of 92 % amongst all chosen catalysts (Fig. 4.1(a)) because of its very fast kinetics. The following order: catalyst-8 > catalyst-1 > catalyst-4 > catalyst-10 > catalyst-3 > catalyst-2 > catalyst-9 > catalyst-6 > catalyst-5 > catalyst-7 > catalyst-11, can be given indicating catalyst-11 with lowest conversion of 83.5 %. Fig. 4.1(b) shows H_2 yield (wt. % of CH_4) over various catalysts with catalyst-8 giving 9.6 % more yield than catalyst 11 under same operating conditions. According to Fig. 4.1(c), there is no abrupt change in H_2 purity when we switch from one catalyst to the other. There is only 2.1 % increase in purity when catalyst-11 is replaced with catalyst-8. According to the mechanism proposed by Soliman et al. [24], rate of SMR reaction R1 is zero for catalyst-2 and the CO_2 produced by R3 is converted to CO by reverse R2.

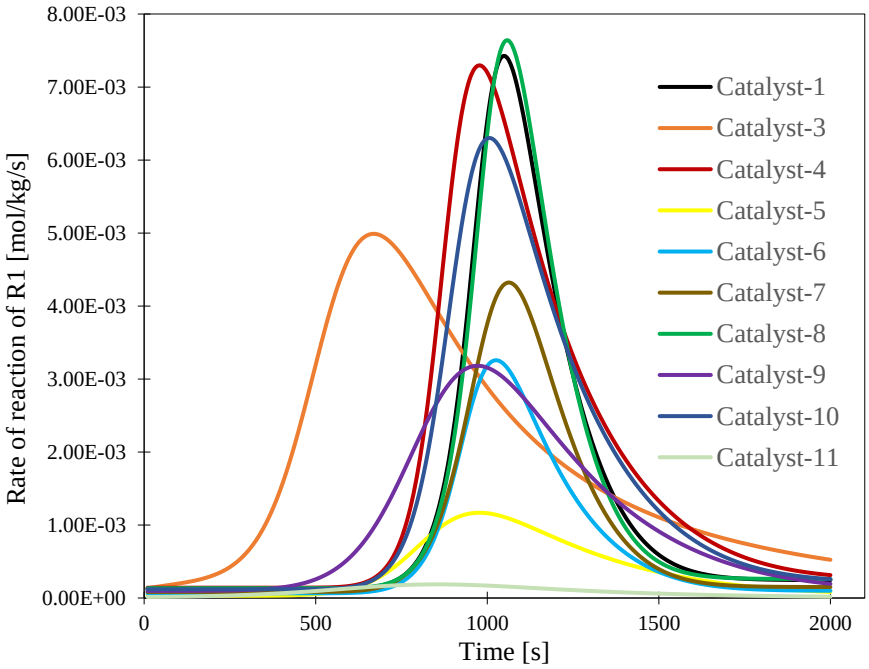

Fig. 4.2. Rate of reaction of R1 as function of time over various catalysts at 973 K, 1 bar, S/C 3.0 and G_s of 3.5 kg m^{-2} s^{-1}.

Fig. 4.3 shows the variation of gas temperature in the middle of the reactor as a function of time. SMR process is highly endothermic in nature and the reactor is being operated in adiabatic mode (q=0), therefore feed is being introduced at a high temperature of 973 K to get better conversion of CH_4. It can be observed from Fig. 4.3 that there is no abrupt change in

temperature of the gas before 750 s for almost every catalyst. But after 750s there is a sudden drop in temperature of gas because of the endothermic reaction R1 and at such high temperature R2 is not active. After 1350 s, gas temperature for catalyst-8 is 850 K showing a drop of 123 K which indicates dominance of R1. Catalyst-2 shows a linear decrease in temperature because R1=0.

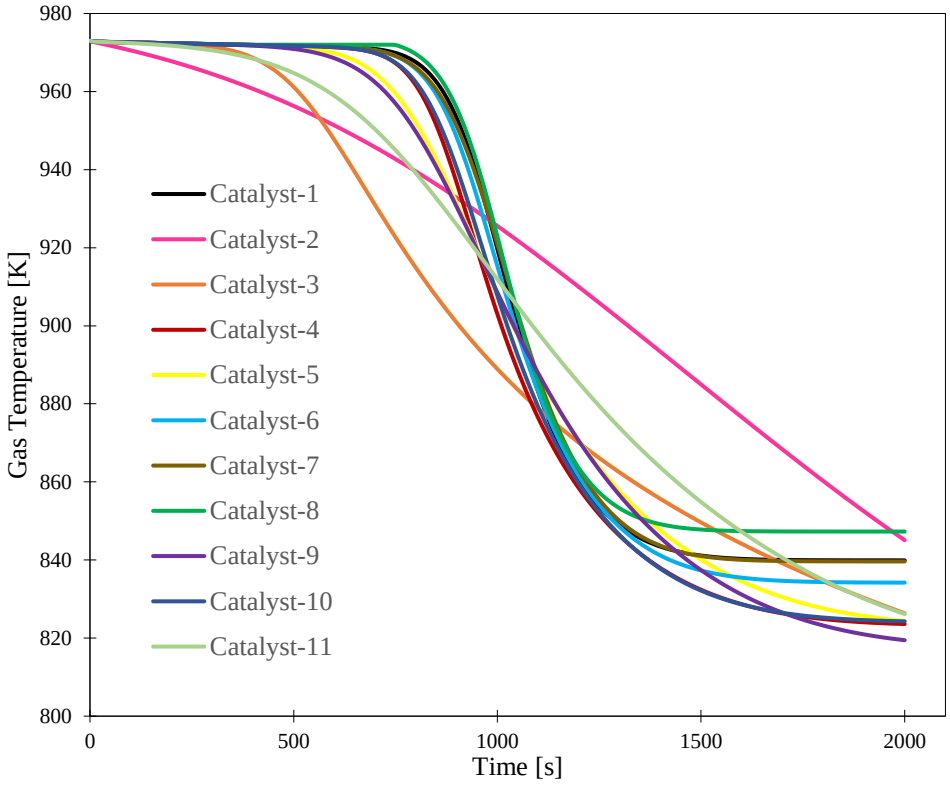

Fig. 4.3. Temperature of gas as function of time over various catalysts at 973 K, 1 bar, S/C 3.0 and G_s of 3.5 kg m^{-2} s^{-1}.

4.1.3 SELECTIVITY OF C-BASED PRODUCTS

Selectivity of carbon containing products in the effluent gas can be modelled according to the following equations;

$$CH_4\ Selectivity\ (\%) = \frac{\dot{n}_{CH_4}}{\left(\dot{n}_{CH_4} + \dot{n}_{CO} + \dot{n}_{CO_2}\right)} \times 100 \quad (4.1)$$

$$CO\ Selectivity\ (\%) = \frac{\dot{n}_{CO}}{\left(\dot{n}_{CH_4} + \dot{n}_{CO} + \dot{n}_{CO_2}\right)} \times 100 \quad (4.2)$$

$$CO_2\ Selectivity\ (\%) = \frac{\dot{n}_{CO_2}}{\left(\dot{n}_{CH_4} + \dot{n}_{CO} + \dot{n}_{CO_2}\right)} \times 100 \quad (6)$$

Where, $\dot{n}_{CH_4}$, $\dot{n}_{CO}$, $\dot{n}_{CO_2}$ correspond to the molar flowrates of CH_4, CO and H_2 at the outlet of

the reactor.

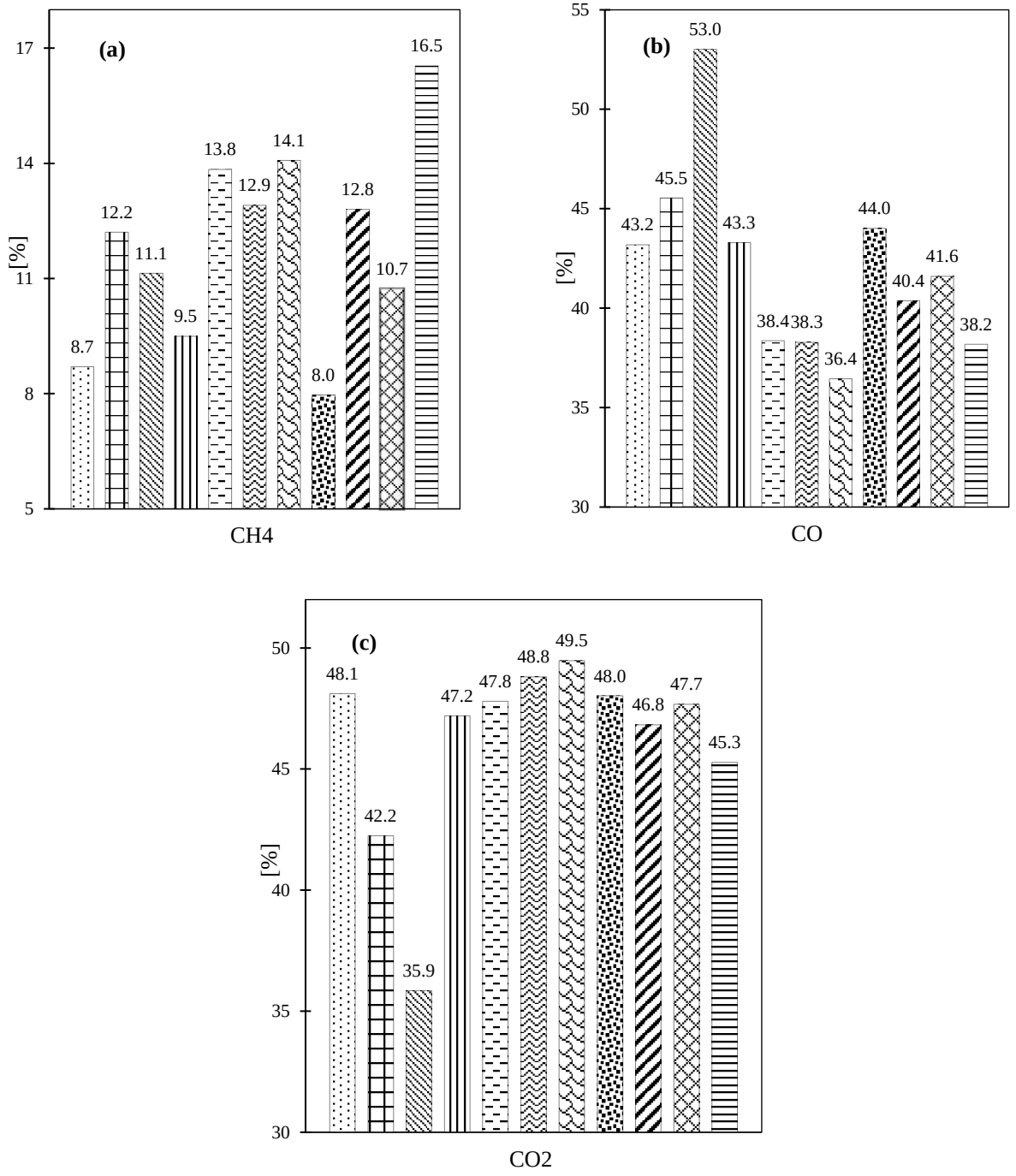

Fig. 4.4. Comparison in terms a) CH_4 selectivity; b) CO selectivity ; c) CO_2 selectivity at 973 K, 1 bar, S/C of 3.0 and G_s of 3.5 kg m^{-2} s^{-1}.

Fig. 4.4 (a-c) shows the comparison between catalysts in terms of selectivity of C-based products, when reformer is allowed to run with identical operating conditions but loaded with different catalyst each time the run is made. In Fig. 4.4 (a), selectivity of CH_4 is maximum for catalyst-11 among all other catalysts due to smaller rate of disappearance for CH_4. Catalys-3 gives the maximum CO selectivity as it is demonstrated in Fig. 4.4(b). Such high value of

selectivity suggests that CO_2 is the primary product with catalyst-3, which is then converted to CO via reverse R2. In Fig. 4.4(c), selectivity of CO_2 is presented with catalyst-7 leading the list with 49.5 % selectivity while catalyst-3 shows a value of 35.9 % under same operational conditions.

It can be inferred from above results that the selectivity of carbon containing products depends on the thermodynamics of reactions. Reaction kinetics can decide which product should be the primary and it will influence the product distribution.

4.1.4 THERMAL EFFICIENCY

The energy efficiency of the reforming process on the basis of LHV as a function of H_2 yield is given as;

$$Thermal\ efficiency\ (\%) = \frac{(moles\ of\ H_2\ produced \times LHV_{H_2})}{(moles\ of\ CH_4\ fed \times LHV_{CH_4})} \times 100 \quad (7)$$

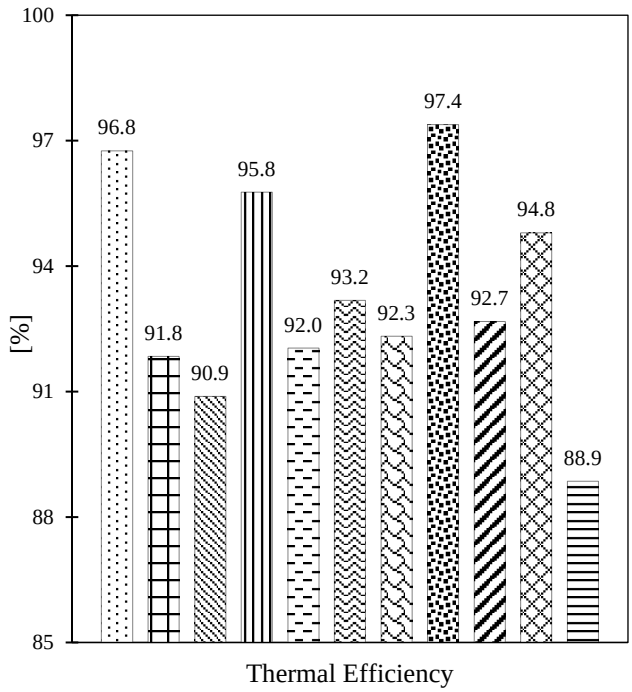

Fig. 4.5. Thermal efficiency of the reformer with various catalysts at 973 K, 1 bar, S/C of 3.0 and G_s of 3.5 kg m^{-2} s^{-1}.

Fig. 4.5 shows the thermal efficiency (%) of the reformer with various catalysts at 973 K, 1 bar, S/C of 3 and with G_s of 3.5 kg m^{-2} s^{-1}. Under the same operating conditions, equilibrium would have given a thermal efficiency of 99.9 %. The higher the S/C and temperature, more

number of moles of H_2 will be produced and higher will be the thermal efficiency. It is evident from Fig. 4.5 that the catalyst-8 gives the maximum thermal efficiency of 97.4% from given set of catalysts because of its ability to give higher H_2 yield at aforementioned operating conditions.

5. CONCLUSION

1-D dimensional heterogeneous mathematical model for an adiabatic fixed bed reactor is constructed and simulated for the SMR process. The first order backward finite difference method was applied to solve the model's system of PDAEs in gPROMS. The sensitivity analysis of the developed packed bed reactor model helped to determine the best operating conditions of temperature, pressure, feed ratio and gas mass flux. The modelling results are found in good agreement with the equilibrium results. Later on, the modelling results are validated against the industrials results. At a fixed pressure, an increase in temperature results an increase in CH_4 disappearance rate, H_2 yield and H_2 purity. At a fixed temperature, lowering the pressure results in improvement of CH_4 conversion. It means SMR process performs best under the conditions of high temperature and low pressure. At 1 bar, when the temperature is increased above 973 K, there is no appreciable increase observed in CH_4 conversion. So under the condition of lower pressure of 1 bar, a temperature of 973 K is chosen as the optimum operating temperature for the SMR process. While taking into consideration the sensitivity of S/C in SMR process owing to its effect on coke deposition and operational cost, S/C of 3 is chosen as optimum to get sufficiently high enough values of CH_4 conversion and H_2 purity. To stay away from equilibrium but to get compositions close to equilibrium a G_s of 3.5 kg m^{-2} s^{-1} is selected. The sensitivity analysis reveals that the SMR process gives the best performance at high temperature, low pressure and at larger values of S/C. The model is then extended to fit kinetics developed over various catalysts to evaluate their performance. Product distribution and thermal efficiency are the criteria to evaluate the performance of the catalysts.

It is concluded from comparison that the catalysts with fast kinetics give better results under given set of operating conditions. In future, 1-D model developed in this work will be upgraded to 2-D model and will be used to simulate the ammonia fertilizer plant. Heat and mass transfer effects inside the pores of the solid particles are not taken into account in the development of the model. In future, a model incorporating the mechanism of transport of gases inside the pores of the catalyst particles can be developed.

6. REFERENCES

[1] Sánchez-Sánchez MC, Navarro RM, Fierro JLG. Ethanol steam reforming over Ni/La–Al_2O_3 catalysts: Influence of lanthanum loading. Catalysis Today 2007;129(3):336-45.

[2] Dincer I, Acar C. Review and evaluation of hydrogen production methods for better sustainability. International Journal of Hydrogen Energy 2015;40(34):11094-111.

[3] Parkinson B, Tabatabaei M, Upham DC, Ballinger B, Greig C, Smart S, et al. Hydrogen production using methane: Techno-economics of decarbonizing fuels and chemicals. International Journal of Hydrogen Energy 2018;43(5):2540-55.

[4] McDowall W, Eames M. Forecasts, scenarios, visions, backcasts and roadmaps to the hydrogen economy: A review of the hydrogen futures literature. Energy Policy 2006;34(11):1236-50.

[5] Sharma S, Ghoshal SK. Hydrogen the future transportation fuel: From production to applications. Renewable and Sustainable Energy Reviews 2015;43:1151-8.

[6] Eliezer D, Eliaz N, Senkov ON, Froes FH. Positive effects of hydrogen in metals. Materials Science and Engineering: A 2000;280(1):220-4.

[7] Dupont V. Steam reforming of sunflower oil for hydrogen gas production. 2007.

[8] Luo M, Yi Y, Wang S, Wang Z, Du M, Pan J, et al. Review of hydrogen production using chemical-looping technology. Renewable and Sustainable Energy Reviews 2018;81:3186-214.

[9] Nikoo MK, Saeidi S, Lohi AJCT, Policy E. A comparative thermodynamic analysis and experimental studies on hydrogen synthesis by supercritical water gasification of glucose. 2015;17(8):2267-88.

[10] Chiron F-X, Patience GS, Rifflart S. Hydrogen production through chemical looping using $NiO/NiAl_2O_4$ as oxygen carrier. Chemical Engineering Science 2011;66(24):6324-30.

[11] Zamaniyan A, Behroozsarand A, Ebrahimi H. Modeling and simulation of large scale hydrogen production. Journal of Natural Gas Science and Engineering 2010;2(6):293-301.

[12] Iulianelli A, Liguori S, Wilcox J, Basile A. Advances on methane steam reforming to produce hydrogen through membrane reactors technology: A review. Catalysis Reviews 2016;58(1):1-35.

[13] Balat M, Balat M. Political, economic and environmental impacts of biomass-based hydrogen. International Journal of Hydrogen Energy 2009;34(9):3589-603.

[14] Muradov NZ, Veziroğlu TN. From hydrocarbon to hydrogen–carbon to hydrogen economy. International Journal of Hydrogen Energy 2005;30(3):225-37.

[15] Fernández JR, Abanades JC, Murillo R, Grasa G. Conceptual design of a hydrogen production process from natural gas with CO_2 capture using a Ca–Cu chemical loop. International Journal of Greenhouse Gas Control 2012;6:126-41.

[16] Farsi M, Shahhosseini H. A modified membrane SMR reactor to produce large-scale syngas: modeling and multi objective optimization. Chemical Engineering and Processing: Process Intensification 2015;97:169-79.

[17] LeValley TL, Richard AR, Fan M. The progress in water gas shift and steam reforming hydrogen production technologies – A review. International Journal of Hydrogen Energy 2014;39(30):16983-7000.

[18] Jones G, Jakobsen JG, Shim SS, Kleis J, Andersson MP, Rossmeisl J, et al. First principles calculations and experimental insight into methane steam reforming over transition metal catalysts. Journal of Catalysis 2008;259(1):147-60.

[19] Guo X, Sun Y, Yu Y, Zhu X, Liu C-j. Carbon formation and steam reforming of methane on silica supported nickel catalysts. Catalysis Communications 2012;19:61-5.

[20] Rydén M, Lyngfelt A, Mattisson T. Chemical-Looping Combustion and Chemical-Looping Reforming in a Circulating Fluidized-Bed Reactor Using Ni-Based Oxygen Carriers. Energy & Fuels 2008;22(4):2585-97.

[21] Akers WW, Camp DP. Kinetics of the methane-steam reaction. AIChE Journal 1955;1(4):471-5.

[22] Numaguchi T, Kikuchi K. Intrinsic kinetics and design simulation in a complex reaction network; steam-methane reforming. Chemical Engineering Science 1988;43(8):2295-301.

[23] Xu J, Froment GF. Methane steam reforming, methanation and water-gas shift: I. Intrinsic kinetics. AIChE Journal 1989;35(1):88-96.

[24] Soliman MA, Adris AM, Al-Ubaid AS, El-Nashaie SSEH. Intrinsic kinetics of nickel/calcium aluminate catalyst for methane steam reforming. Journal of Chemical Technology & Biotechnology 1992;55(2):131-8.

[25] Luna AC, Becerra AJRK, Letters C. Kinetics of methane steam reforming on a Ni on alumina-titania catalyst. 1997;61(2):369-74.

[26] Hou K, Hughes R. The kinetics of methane steam reforming over a Ni/α-Al_2O catalyst. Chemical Engineering Journal 2001;82(1):311-28.

[27] McGreavy C, Newmann M. Development of a mathematical model of a steam methane

reformer. Institution of Electrical Engineering, Conference on the Industrial Applications of Dynamic Modelling. 1969.

[28] Singh CPP, Saraf DN. Simulation of Low-Temperature Water-Gas Shift Reactor. Industrial & Engineering Chemistry Process Design and Development 1980;19(3):393-6.

[29] Xu J, Froment GF. Methane steam reforming: II. Diffusional limitations and reactor simulation. AIChE Journal 1989;35(1):97-103.

[30] Soliman MA, El-Nashaie SSEH, Al-Ubaid AS, Adris A. Simulation of steam reformers for methane. Chemical Engineering Science 1988;43(8):1801-6.

[31] Murty CVS, Murthy MVK. Modeling and simulation of a top-fired reformer. Industrial & Engineering Chemistry Research 1988;27(10):1832-40.

[32] Plehiers PM, Froment GF. Coupled simulation of heat transfer and reaction in a steam reforming furnace. Chemical Engineering & Technology 1989;12(1):20-6.

[33] Yu Z, Cao E, Wang Y, Zhou Z, Dai Z. Simulation of natural gas steam reforming furnace. Fuel Processing Technology 2006;87(8):695-704.

[34] Shayegan J, Hashemi MMYM, Vakhshouri K. Operation of an industrial steam reformer under severe condition: A simulation study. The Canadian Journal of Chemical Engineering 2008;86(4):747-55.

[35] Ebrahimi H, Mohammadzadeh JSS, Zamaniyan A, Shayegh F. Effect of design parameters on performance of a top fired natural gas reformer. Applied Thermal Engineering 2008;28(17):2203-11.

[36] Olivieri A, Vegliò F. Process simulation of natural gas steam reforming: Fuel distribution optimisation in the furnace. Fuel Processing Technology 2008;89(6):622-32.

[37] Hossain MM, de Lasa HI. Reactivity and stability of Co-Ni/Al_2O_3 oxygen carrier in multicycle CLC. AIChE Journal 2007;53(7):1817-29.

[38] Jin H, Ishida M. Reactivity Study on Natural-Gas-Fueled Chemical-Looping Combustion by a Fixed-Bed Reactor. Industrial & Engineering Chemistry Research 2002;41(16):4004-7.

[39] Rydén M, Lyngfelt A, Mattisson T. Synthesis gas generation by chemical-looping reforming in a continuously operating laboratory reactor. Fuel 2006;85(12):1631-41.

[40] Ávila-Neto CN, Dantas SC, Silva FA, Franco TV, Romanielo LL, Hori CE, et al. Hydrogen production from methane reforming: Thermodynamic assessment and autothermal reactor design. Journal of Natural Gas Science and Engineering

2009;1(6):205-15.

[41] Freitas ACD, Guirardello R. Thermodynamic analysis of methane reforming with CO_2, CO_2+H_2O, CO_2+O_2 and CO_2+air for hydrogen and synthesis gas production. Journal of CO_2 Utilization 2014;7:30-8.

[42] Özkara-Aydınoğlu Ş. Thermodynamic equilibrium analysis of combined carbon dioxide reforming with steam reforming of methane to synthesis gas. International Journal of Hydrogen Energy 2010;35(23):12821-8.

[43] Li Y, Wang Y, Zhang X, Mi Z. Thermodynamic analysis of autothermal steam and CO_2 reforming of methane. International Journal of Hydrogen Energy 2008;33(10):2507-14.

[44] Smith JM. Introduction to chemical engineering thermodynamics. ACS Publications; 1950.

[45] Lutz AE, Bradshaw RW, Keller JO, Witmer DE. Thermodynamic analysis of hydrogen production by steam reforming. International Journal of Hydrogen Energy 2003;28(2):159-67.

[46] Seo YS, Shirley A, Kolaczkowski ST. Evaluation of thermodynamically favourable operating conditions for production of hydrogen in three different reforming technologies. Journal of Power Sources 2002;108(1):213-25.

[47] Farshchi Tabrizi F, Mousavi SAHS, Atashi H. Thermodynamic analysis of steam reforming of methane with statistical approaches. Energy Conversion and Management 2015;103:1065-77.

[48] Rostrup-Nielsen JR, Sehested J, Nørskov JK. Hydrogen and synthesis gas by steam- and C02 reforming. Advances in Catalysis. Academic Press; 2002, p. 65-139.

[49] Hoang DL, Chan SH, Ding OL. Kinetic and modelling study of methane steam reforming over sulfide nickel catalyst on a gamma alumina support. Chemical Engineering Journal 2005;112(1):1-11.

[50] Oliveira ELG, Grande CA, Rodrigues AE. Methane steam reforming in large pore catalyst. Chemical Engineering Science 2010;65(5):1539-50.

[51] Oliveira ELG, Grande CA, Rodrigues AE. Steam methane reforming in a Ni/Al_2O_3 catalyst: Kinetics and diffusional limitations in extrudates. The Canadian Journal of Chemical Engineering 2009;87(6):945-56.

[52] Halabi MH, de Croon MHJM, van der Schaaf J, Cobden PD, Schouten JC. Intrinsic kinetics of low temperature catalytic methane–steam reforming and water–gas shift over $Rh/Ce_{\alpha}Zr_{1-\alpha}O_2$ catalyst. Applied Catalysis A: General 2010;389(1):80-91.

[53] Kanhari C, Vatanatham T, Limtrakul S. Kinetic Rates of Steam-Methane Reforming over Ni / Al_2O_3 catalyst. Kasetsart Engineering Journal 2013;85(1):53-62.

[54] Obradović A, Likozar B, Levec J. Steam Methane Reforming over Ni-based Pellet-type and Pt/Ni/Al_2O_3 Structured Plate-type Catalyst: Intrinsic Kinetics Study. Industrial & Engineering Chemistry Research 2013;52(38):13597-606.

[55] Abbas SZ, Dupont V, Mahmud T. Kinetics study and modelling of steam methane reforming process over a NiO/Al_2O_3 catalyst in an adiabatic packed bed reactor. International Journal of Hydrogen Energy 2017;42(5):2889-903.

[56] Yagi S, Kunii D, Wakao N. Studies on axial effective thermal conductivities in packed beds. AIChE Journal 1960;6(4):543-6.

[57] Edwards MF, Richardson JF. Gas dispersion in packed beds. Chemical Engineering Science 1968;23(2):109-23.

[58] Geankoplis CJN, MA. Transport Processes and Unit Operations. Allyn and Bacon. 1995.

[59] Handley D, Heggs PJ. The effect of thermal conductivity of the packing material on transient heat transfer in a fixed bed. International Journal of Heat and Mass Transfer 1969;12(5):549-70.

7. APPENDICES

7.1 APPENDIX A

The kinetic rate equations and kinetic parameters used in the reactor model:

$$R_1 = \frac{k_1}{p_{H_2}^{2.5}}\left(p_{CH_4}p_{H_2O} - \frac{p_{H_2}^3 p_{CO}}{K_I}\right)\left(\frac{1}{\Omega^2}\right) \quad \text{(A.1)}$$

$$\mathrm{R}_2 = \frac{k_3}{p_{H_2}}\left(p_{co}p_{H_2O} - \frac{p_{H_2}p_{CO}}{K_{\mathrm{II}}}\right)\left(\frac{1}{\Omega^2}\right) \quad \text{(A.2)}$$

$$R_3 = \frac{k_2}{p_{H_2}^{3.5}}\left(p_{CH_4}p_{H_2O}^2 - \frac{p_{H_2}^4 p_{CO_2}}{K_{III}}\right)\left(\frac{1}{\Omega^2}\right) \quad \text{(A.3)}$$

$$\Omega = 1 + K_{CO}p_{CO} + K_{H_2}p_{H_2} + K_{CH_4}p_{HCH_4} + K_{H_2O}\frac{p_{H_2O}}{p_{H_2}} \quad \text{(A.4)}$$

$$R_1 = \frac{k_1}{p_{H_2}^{1.25}}\left(p_{CH_4}\, p_{H_2O}^{0.5} - \frac{p_{H_2}^3 p_{CO}}{K_I\, p_{H_2O}^{0.5}}\right)\left(\frac{1}{\Omega^2}\right) \quad \text{(A.5)}$$

$$\mathrm{R}_2 = \frac{k_2}{p_{H_2}^{0.5}}\left(p_{CO}\, p_{H_2O}^{0.5} - \frac{p_{H_2}p_{CO_2}}{K_{\mathrm{II}}\, p_{H_2O}^{0.5}}\right)\left(\frac{1}{\Omega^2}\right) \quad \text{(A.6)}$$

$$R_3 = \frac{k_3}{p_{H_2}^{1.75}}\left(p_{CH_4}\, p_{H_2O} - \frac{p_{H_2}^4 p_{CO_2}}{K_{III}\, p_{H_2O}}\right)\left(\frac{1}{\Omega^2}\right) \quad \text{(A.7)}$$

$$\Omega = 1 + K_{CO}\, p_{CO} + K_{H_2}\, p_{H_2}^{0.5} + K_{H_2O}\frac{p_{H_2O}}{p_{H_2}} \quad \text{(A.8)}$$

$$R_1 = \frac{k_1}{p_{H_2}^{2.5}}\left(p_{CH_4}p_{H_2O} - \frac{p_{H_2}^3 p_{CO}}{K_I}\right) \times \Omega_1\Omega_S \quad \text{(A.9)}$$

$$\mathrm{R}_2 = \frac{k_2}{p_{H_2}}\left(p_{CO}p_{H_2O} - \frac{p_{H_2}p_{CO_2}}{K_{\mathrm{II}}}\right) \times \Omega_1\Omega_S \quad \text{(A.10)}$$

$$R_3 = \frac{k_3}{p_{H_2}^{3.5}}\left(p_{CH_4}p_{H_2O}^2 - \frac{p_{H_2}^4 p_{CO_2}}{K_{III}}\right) \times \Omega_1\Omega_S \quad \text{(A.11)}$$

$$\Omega_1 = \frac{1}{1 + K_{CH_4} p_{CH_4} / {p_{H_2}}^{0.5} + K_{CO} p_{CO} + K_{CO_2} p_{CO_2} + K_{H_2} p_{H_2}} \quad \text{(A.12)}$$

$$\Omega_S = \frac{1}{1 + K_{H_2O} p_{H_2O} / p_{H_2} + K_{H_2} p_{H_2}} \quad \text{(A.13)}$$

$$K_I = exp\left(\frac{-26830}{T_s} + 30.114\right) \quad \text{(A.14)}$$

$$K_{II} = exp\left(\frac{4400}{T_s} - 4.036\right) \quad \text{(A.15)}$$

$$K_{III} = K_I K_{II} \quad \text{(A.16)}$$

$$k_j = k_{oj} exp\left(\frac{-E_j}{R_g T}\right) \quad \text{(A.17)}$$

$$K_i = K_{oi} exp\left(\frac{-\Delta H_i}{R_g T}\right) \quad \text{(A.18)}$$

7.2 APPENDIX B

Physical properties are estimated by using the following empirical correlations:

Effective thermal conductivity is given as [56];

$$\frac{\lambda_z^f}{\lambda_g} = \frac{\lambda_z^o}{\lambda_g} + 0.75 Pr Re_p \quad \text{(B.1)}$$

$$\frac{\lambda_z^o}{\lambda_g} = \varepsilon_b + \frac{1 - \varepsilon_b}{0.139\varepsilon_b - 0.0339 + \left(\frac{2}{3}\right)\lambda_g/\lambda_s} \quad \text{(B.2)}$$

Axial mass dispersion coefficient is defined is expressed as [57];

$$D_z = 0.73 D_m + \frac{0.5 u d_p}{1 + 9.49\, D_m / u d_p} \quad \text{(B.3)}$$

The mass transfer coefficient is given by the following relation [58];

$$k_{g,i} = j_{D,i} Re_p Sc_i^{1/3} \frac{D_i}{d_p} \quad \text{(B.4)}$$

$$k_{g,i} = j_{D,i} {Re_p}^{-0.82} + 0.365 Sc_i^{-0.398} \quad \text{(B.5)}$$

The dimensionless numbers are given as;

$$Re_p = \frac{\rho_g u d_p}{\mu} \; ; \; 0.01 < Re_p < 1500 \quad \text{(B.6)}$$

$$Sc_i = \frac{\mu}{\rho_g D_i} \; ; \; 0.6 < Sc < 7000 \, , 0.25 < \varepsilon_b < 0.96 \quad \text{(B.7)}$$

Heat transfer coefficient and its dimensionless numbers are given by the following expressions [58, 59];

$$h_f = j_H \frac{C_{pg} G_s}{Pr^{2/3}} \quad \text{(B.8)}$$

$$j_H = 0.91 {Re_p}^{-0.51} \psi \; ; \; 0.01 < Re_p < 50 \quad \text{(B.9)}$$

$$j_H = 0.61 {Re_p}^{-0.41} \psi \; ; \; 50 < Re_p < 1000 \quad \text{(B.10)}$$

$$Pr = \frac{C_{pg} \mu_g}{\lambda_g} \quad \text{(B.11)}$$